Picosecond-laser-induced transient dynamics of phonons in GaP and ZnSe

W. E. Bron*
Department of Physics, Indiana University, Bloomington, Indiana 47405

J. Kuhl
Max-Planck-Institut für Festkörperforschung, D-7000 Stuttgart 80, West Germany

B. K. Rhee†
Department of Physics, Indiana University, Indiana 47405

(Received 14 February 1986; revised manuscript received 23 June 1986)

We report on the vibrational and electronic response of GaP and ZnSe subjected to resonant coherent Raman excitation by picosecond-laser light and probed with time-resolved coherent anti-Stokes Raman scattering. Previously reported measurements of the dephasing time of longitudinal optical phonons and of the third-order nonlinear electronic susceptibility in GaP are extended to include ZnSe. The temperature dependence of the dephasing time of coherent phonons is determined and is compared to that obtained from spontaneous (incoherent) Raman scattering. The experimental and analytical methods are reported in detail.

I. INTRODUCTION

The advent of dual synchronously pumped dye lasers which produce synchronized trains of pulses with picosecond (and subpicosecond) duration at two different wavelengths, has greatly expanded the range and detail of the study of the interaction of coherent laser light with condensed matter. As examples of such applications we report the generation of near-zone-center coherent optical phonons in GaP and ZnSe through coherent Raman excitation (CRE), and the subsequent dynamics of the coherent longitudinal optical (LO) phonon state, plus the response of the electronic system to nonlinear excitation. These investigations were carried out directly in the time domain through time-resolved coherent anti-Stokes Raman scattering (TRCARS). A part of these results have been previously reported[1–4] in the form of short communications, in recognition of the rapid rate at which this field is expanding.

In the present paper we present additional results on the temperature dependence of the decay of transverse optical (TO) phonons in both GaP and ZnSe, on measurements of the temperature dependence of the dephasing time for LO phonons in ZnSe, plus measurements of the third-order nonlinear electronic susceptibility $\chi^{(3)}$ for ZnSe. Also presented is a theoretical basis for the measurements (Sec. II), the details of the experimental techniques (Sec. III), and an analysis of the experimental results (Sec. IV).

Coherent Raman excitation (CRE) and coherent anti-Stokes Raman scattering (CARS) are particular forms of nonlinear mixing of laser fields.[5] Two electromagnetic fields $\mathbf{E}_l$ and $\mathbf{E}_s$, with photon energies $\hbar\omega_l$ and $\hbar\omega_s$ and wave vectors $\mathbf{k}_l$, $\mathbf{k}_s$, can in general give rise to a series of nonlinear interactions in a solid. One interaction leads to a virtual excitation of the electronic system at a frequency $\omega_l-\omega_s$ [see Fig. 1(a)]. Of particular interest here is the case in which $\omega_l-\omega_s$ corresponds to a Raman active vibrational excitation [Fig. 1(b)]. In the resultant CRE, the energy $\hbar(\omega_l-\omega_s)$ and wave vector $\mathbf{q}=\mathbf{k}_l-\mathbf{k}_s$ of the active mode are in the ideal case exactly specified,[6] and the phase space available to the excited vibrations is severely limited. In this sense it differs markedly from stimulated and spontaneous Raman scattering for which the available phase space is much larger. Thus, the occupation probabilities of the components of the coherent state produced through CRE may be very high as compared to those of incoherent Raman excitation. Generation of intense coherent oscillations by CRE was first described for molecular systems by Garmire *et al.*[7] Large amplitude coherent excitation of lattice vibrations was soon thereafter described by Giordmaine and Kaiser.[8]

The coherent excitation may be probed by a third laser field $\mathbf{E}_p$ whose energy $\hbar\omega_p$ is taken for convenience to be $\hbar\omega_l$ [see Figs. 1(a) and 1(b)]. The nonlinear interaction of this field, with the coherent lattice vibrations results in yet another nonlinear polarization[9] which drives an electromagnetic field with energy $\hbar\omega_c=\hbar(2\omega_l-\omega_s)$. It is fur-

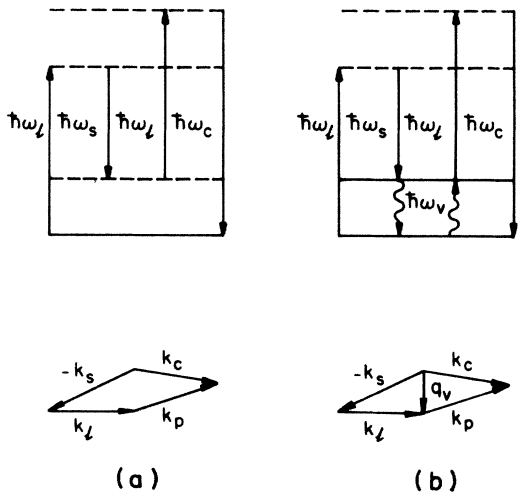

FIG. 1. Energy and k-vector conservation for the three-wave-mixing signal associated with CARS. Figure 1(a) illustrates the nonresonant electronic contribution, Fig. 1(b) the resonant Raman process.

ther required through wave vector conservation (the phase-matching condition) that $\mathbf{k}_c=\mathbf{k}_p+\mathbf{k}_l-\mathbf{k}_s$, where $\mathbf{k}_p$ and $\mathbf{k}_c$ are the wave vectors associated with the probe pulse and the anti-Stokes pulse, respectively. The probe technique, clearly involves coherent anti-Stokes Raman scattering, giving rise to the CARS designation for the entire nonlinear process.

II. THEORETICAL BACKGROUND

The coherent phonon state mentioned in the previous section is defined by a superposition of states of different occupation probabilities, but whose component states have, at least initially, a fixed relative phase relationship among each other. The resultant excitation of the solid resembles most closely a classical harmonic oscillator.[10]

We first concentrate on the coherent LO phonon state and delay further discussion of TO phonons until Sec. V. We describe the coherent LO phonon state in terms of the following classical equation of motion for the coherent amplitude $\langle Q\rangle$:[11]

$$\mu(\ddot{Q}^{+}+\Gamma\dot{Q}^{+}+\omega_{\mathrm{LO}}^2 Q^{+})=\hat{\mathbf{q}}\cdot\left[\bar{R}\mathbf{E}_l^{+}\mathbf{E}_s^{-}-\frac{4\pi e^{*}}{\epsilon_\infty}\mathbf{P}_{\mathrm{NL}}^{+}\right]. \tag{1}$$

In Eq. (1), μ is the reduced lattice mass, Γ a phenomenological damping rate, ω_{LO} phonon frequency, $\hat{\mathbf{q}}$ the unit polarization vector of LO phonon, ϵ_∞ the high frequency dielectric constant, $\bar{R}$ the appropriate Raman tensor, e^{*} the effective lattice charge, $\mathbf{P}_{\mathrm{NL}}$ a nonlinear polarization and the superscript plus refers to the Fourier component $\exp[i(\mathbf{k}\cdot\mathbf{x}-\omega t)]$ and minus refers to its complex conjugate. Equation (1) implies that the amplitude $\langle Q\rangle$ of the coherent state is driven by a force involving a Raman interaction and by a force associated with the longitudinal component of a nonlinear polarization which acts as a depolarization field. If only the lowest order of P_{NL} (i.e., of second order in the fields) is considered, the driving force, $F(j)$, in Eq. (1) is reduced to

$$F\{j\}=R_A\{j\}E_l^{+}E_s^{-}, \tag{2}$$

where $R_A\{j\}=(\bar{R}_A\cdot\hat{\mathbf{q}})\hat{l}\hat{\mathbf{s}}$ and $\bar{R}_A=\bar{R}-(4\pi e^{*}/\epsilon_\infty)\bar{\chi}^{(2)}$. Here, $\{j\}$ is an index for the geometrical configuration of the polarization of the two l- and s-laser beams with respect to the crystal axis, $\bar{\chi}^{(2)}$ the second-order nonlinear susceptibility tensor, and $\hat{l}$ and $\hat{\mathbf{s}}$ are the unit polarization vectors of the fields E_l, E_s (see Fig. 2). According to the theoretical and experimental results of Ushioda *et al.*,[12] R and R_A can be measured separately by comparing the intensity ratio of the Raman scattering strength from LO to that from TO phonons. However, we point out that their experimental results appear to be in contradiction to the corresponding results of Calleja *et al.*[13]

The experimentally observable parameter in the CARS experiment is the intensity of the TRCARS signal at the energy $\hbar\omega_c=\hbar(2\omega_l-\omega_s)$. This intensity is proportional to the absolute square of the nonlinear polarization induced in the vibrational and electronic systems due to the three laser fields $\mathbf{E}_l$, $\mathbf{E}_s$, and $\mathbf{E}_p$. Thus an expression for this quantity can be written as[3]

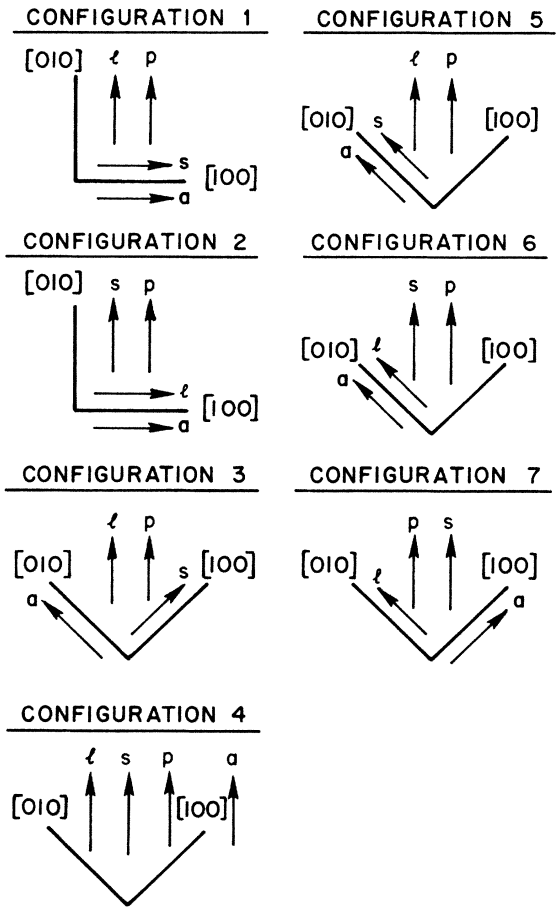

FIG. 2. Polarization configurations. The letters in the diagram refer to the polarization of the l-, s-, and p-laser beams and a to the polarization direction of the analyzer placed in the CARS beam.

$$I_c(\Delta t)=AS\int_{-\infty}^{\infty}dt\,|\,\mathbf{E}_p^{+}(t+\Delta t)\times[N(\bar{R}_A\cdot\hat{\mathbf{q}})Q^{+}(t)+\bar{\chi}_{\mathrm{eff}}^{(3)}\mathbf{E}_l^{+}(t)\mathbf{E}_s^{-}(t)]\,|^2, \tag{3}$$

where $A=2\pi\omega_c^2L^2/c\epsilon_c$, $S=\sin^2(\Delta\mathbf{k}\cdot\mathbf{L}/2)/(\Delta\mathbf{k}\cdot\mathbf{L}/2)^2$, and $\Delta\mathbf{k}=\mathbf{k}_c-(\mathbf{k}_l+\mathbf{k}_p-\mathbf{k}_s)$.

In Eq. (3), the factor S goes to unity as the phase mismatch $\Delta\mathbf{k}$ goes to zero, L is the length of the spatial overlap within the sample of all three laser fields, c is the speed of light, ϵ_c the dielectric constant of the medium at ω_c, Δt is the temporal difference between the probe pulse and that of $\mathbf{E}_l$ and $\mathbf{E}_s$ (which are set as close as possible to the exact time overlap $\delta t=0$), N is the number of primitive cells per unit volume, $\bar{\chi}_{\mathrm{eff}}^{(3)}$ is the effective third-order nonlinear electronic susceptibility.

It is clear from Eq. (3) that there are two contributions to $I_c(\Delta t)$, i.e., one due to the response of the lattice and one to the response of the electronic system and that the relative contributions of the phonon part to the electronic part depend on the geometrical configuration $\{j\}$ of the polarization direction of the three laser beams and that of an analyzer (placed in the CARS field) with respect to the crystal axes. The explicit expressions for the response of

the vibrational and electronic systems, for the seven possible configurations for the present case (see Fig. 2), are presented in the Appendix. Equivalent expressions for the CARS intensity in the spectral (rather than the temporal) domain have been described for the zinc-blende structure with inversion symmetry by Levenson and Bloembergen[9] and without inversion symmetry by Flytzanis *et al.*[14] The parameter $\chi^{(3)}$ may be complex, and the lattice term is purely imaginary at resonance, i.e., at $\omega_{LO}-\omega_l-\omega_s$. Thus interference between these contributions are expected. We show in Sec. IV that the individual contributions to $I_c(\Delta t)$ can never the less be separated out, and that all the components of the complex $\chi^{(3)}$ can be recovered from the experimental data.

The components of the coherent phonon state described above are expected to dephase relative to each other after the excitation fields $\mathbf{E}_l$ and $\mathbf{E}_s$ cease. In general, phonon dephasing in solids results from scattering at boundaries, lattice imperfections, carriers, or through population decay brought about by anharmonic interactions. Near-zone-center LO phonons possess, however, nearly zero-group velocities so that their generation in the bulk of the solid (as is done here) eliminates boundary scattering as an active dephasing mode. Impurity scattering may also be neglected in high-quality crystals. We demonstrate in Sec. V that the experimental results support this supposition. Carrier scattering may also be neglected for observations in excess of a few picoseconds after carrier generation. This conclusion stems from the recently obtained knowledge[15] that hot carriers decay in this time scale to an electron-hole plasma at a conduction-band minimum. On the assumption that the carrier effective mass m^* is approximately 0.25 that of the free electron mass, it is easy to show that the LO phonon off which the plasma can scatter (and conserve energy and crystal momentum) must have a wave vector of the order of 10^5 cm^{-1}, which is 2 orders of magnitude greater than the wave vector of the LO phonons under investigation here (see Sec. III). Thus, contrary to the assumptions we made in Ref. 2, we now assume that, under our experimental conditions, only anharmonic phonon decay can be expected to contribute to the dephasing time.

At low temperature and phonon frequencies ω such that $\hbar\omega \gg k_B T$, three-phonon anharmonic decay processes should dominate. It is interesting to note that the magnitudes of the anharmonic scattering rate Γ and its temperature dependence, predicted theoretically for the dephasing through anharmonic decay of a coherent phonon state[16] and separately for the dephasing through anharmonic decay of incoherent phonons,[17] are identical in every way. The most general expression for Γ being

$$\Gamma(q,\omega_q)=2\pi \sum_{q',q''} \frac{|V_{qq'q''}|^2}{\omega_q\omega_{q'}\omega_{q''}}\delta(\omega_q-\omega_{q'}-\omega_{q''}) \times[1+n_T(\omega_{q'})+n_T(\omega_{q''})] . \quad (4)$$

In Eq. (4), q,q',q'' refer to the wave vectors of the phonons involved, $V_{qq'q''}$ is the appropriate matrix element for the third-order anharmonic process, and $n_T(\omega_{q'}) = [\exp(\hbar\omega_{q'}/k_B T)-1]^{-1}$.

It has been generally accepted that the phonon dephasing time, $T_2/2$, obtained from TRCARS measurements, is related to the spectral linewidth $\delta\nu$ (in cm^{-1}) of the incoherent spontaneous Raman scattering cross section. The relation is $T_2/2=(2\pi\delta\nu)^{-1}$ provided that the Raman scattering line shape is homogenously broadened,[18] i.e., it possesses a Lorentzian profile. Moreover, if the line shape is Lorentzian one would predict that in the temporal domain the amplitude of the coherent phonon state decays exponentially. Thus one would predict that the phonon contribution to $I_c(\Delta t)$ (which is proportional to $\langle Q\rangle^2$) decays as $\exp(-2t/T_2)$.

III. EXPERIMENTAL TECHNIQUE

The experimental apparatus is depicted in Fig. 3; it has been briefly described in Ref. 1. Nearly 100-ps duration pulses at a repetition rate of 76.5 MHz are produced by an acousto-optically mode-locked argon-ion laser with an average output power of about 700 mW (at 514 nm). The pulse train is split into equally intense pump beams which excite two identical dye lasers equipped with 80% output couplers and intracavity two-plate birefringent variable-frequency filters. The two dye lasers are driven synchronously such that two pulse trains emerge (again at a 76.5-MHz repetition rate), each with pulses of duration of about 4-ps autocorrelation widths and with an average power of 30–40 mW ($\sim$180 W peak power, $\sim$0.5 nJ energy per pulse) and spectral bandwidth of 6–8 cm^{-1}. Either laser can be tuned such that the difference frequency ranges from 0 to 4000 cm^{-1}, if Rhodamine-110, Rhodamine-6G, or DCM are employed as laser dyes. The

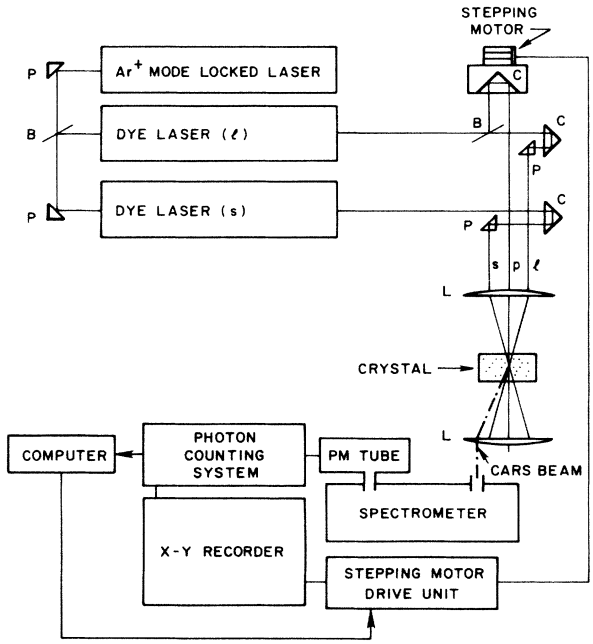

FIG. 3. Experimental apparatus for TRCARS. The letters in the diagram refer to *B*: beam splitter, *C*: corner cube, *P*: right angle prism *L*: lens and *l,s*, and *p* to the laser beams discussed in the text.

laser frequencies chosen were such that $\omega_l-\omega_s=\omega_{LO}$ or ω_{TO} which for GaP is $\omega_{LO}=403$ cm^{-1}, $\omega_{TO}=367$ cm^{-1} and for ZnSe is $\omega_{LO}=251$ cm^{-1}, $\omega_{TO}=204$ cm^{-1}. The total optical path length of the l- and s-laser branches are identical so that the pulses split at the beam splitter reunite in the sample at the same time (and within an approximately $50\times50\times50$ μm^3 overlap volume within the bulk of the sample). The l- and s-laser wave vectors correspond to a forward scattering geometry such that the magnitude of the phonon wave vector was $\lesssim3000$ cm^{-1}; i.e., about 2 orders of magnitude less than that required for scattering by an electron-hole plasma.

Samples of GaP and ZnSe of dimension a few millimeter on each edge were held over a range of temperatures from 5–300 K to within an accuracy of about ±0.5 K. The GaP sample contains about 4×10^{16} cm^{-3} isoelectronic nitrogen impurities, whereas the impurity content of the ZnSe crystal is unknown. Standard measurements were also performed on the linewidth of the incoherent spontaneous Raman scattering intensity. For this purpose the cw argon ion laser line at 514 nm and backward scattering geometries are used.

In the TRCARS measurements, a part of the l-laser beam was split off to produce a probe pulse train whose total optical path length to the crystal could be varied through an optical delay (see translator in Fig. 3) such that its arrival at the sample preceded or lagged behind the arrival time of pulses from the l and s lasers. The nominal resolution of the corresponding temporal delay Δt was of the order of tens of femtoseconds, i.e., much shorter than the pulse widths. Every effort was made before each run to set the temporal mismatch δt between conjugate pulses from the l- and s-laser beams equal to zero. Nevertheless some slight deviation from zero did usually occur. This deviation together with the temporal profiles of the laser pulses $E_l(t)$, $E_s(t)$, and $E_p(t)$ influence the determination of $\chi^{(3)}$. The profiles are extracted from autocorrelation and cross correlation measurements[5] and from the nonresonant electronic contribution to $I_c(\Delta t)$. The resultant temporal profiles are discussed in Sec. IV below.

IV. EXPERIMENTAL RESULTS AND ANALYSIS

A. Generation and dephasing of coherent LO phonons

Figure 4 illustrates typical normalized TRCARS intensities as a function of the time delay Δt between the two pump beams (E_l,E_s) relative to the probe beam (E_p) for the case of GaP held at 4.2 and 300 K, and with $\omega_l-\omega_s=\omega_{LO}$ so that the coherent LO phonon state is excited. The two components of $I_c(\Delta t)$ are clearly visible. The first component near $\Delta t=0$, which can be independently observed when $\omega_l-\omega_s\neq\omega_{LO}$, is a slightly asymmetric "bell-shaped" curve as displayed as the dashed-dotted curve in Fig. 5 (see also Fig. 1 of Ref. 2). This component of $I_c(\Delta t)$ is attributed to the nonlinear, electronic response of the crystal $I_c^e(\Delta t)$. The remaining part of $I_c(\Delta t)$ decreases exponentially with delay time for $\Delta t\gg0$ and can be observed to do so over several orders of magnitude. Thus for these experimental conditions the time interval over which the coherent phonon state is observed to decay is long compared to the time interval over which the purely electronic signal is observed. The slope of the "phonon" part of $I_c(\Delta t)$ is then equal to the dephasing time $T_2/2$. The experimental results on the temperature dependences of $T_2/2$ for coherent LO phonon dephasing in GaP and ZnSe are indicated as solid circles in Figs. 6 and 7, respectively.

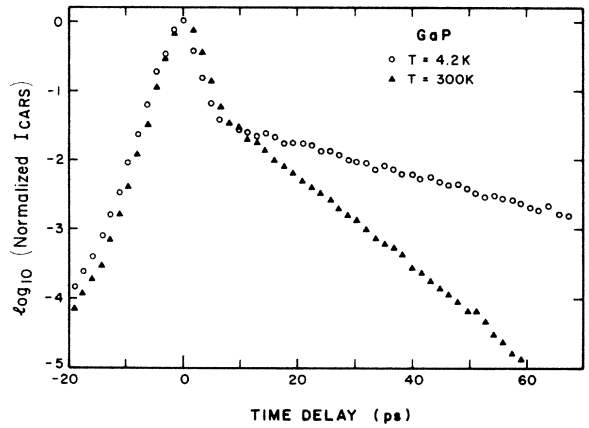

FIG. 4. Temporal evolution of the CARS intensity at the LO phonon resonance of GaP for sample temperatures of 4.2 and 300 K.

Similar measurements for the dephasing time of coherent TO phonons were also attempted by setting $\omega_l-\omega_s=\omega_{TO}$. For all temperatures in both GaP and ZnSe we find only the bell-shaped electronic response. We conclude that the dephasing time for coherent TO phonons is less than the lower limit of our temporal resolution (1–2 ps), i.e., it corresponds to a steeper (negative) slope than that of the positive Δt component of the purely electronic response and is, therefore, hidden.

The temperature dependence of $T_2/2$ has also been determined through linewidth measurements of the spontaneous Raman scattering intensity. The results are displayed in Figs. 6 and 7 as crosses for LO phonons in GaP, as solid triangles for TO phonons in GaP, as open

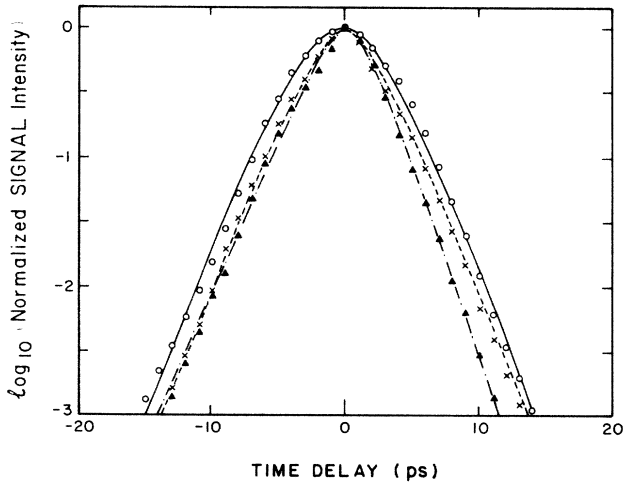

FIG. 5. Temporal evolution of the intensity of the autocorrelation signal (dashed line); of the cross correlation signal (solid line); and of the three-wave-mixing signal (dotted line).

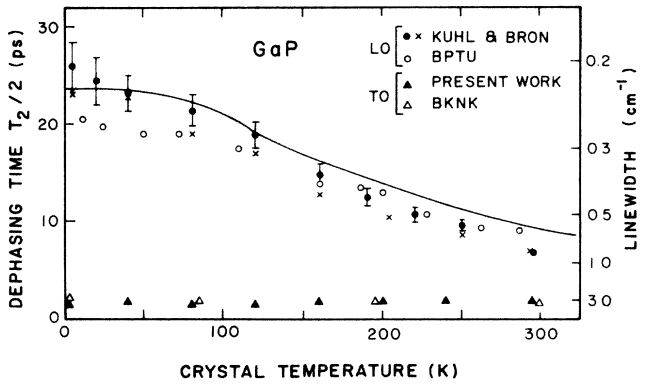

FIG. 6. Temperature dependence of $T_2/2$ and of the Raman linewidths of LO and TO phonons in GaP. The solid circles and crosses refer to data from Ref. 2. The open circles and open triangles refer to data from Refs. 19 and 20, respectively.

circles and crosses for LO phonons in ZnSe, and as solid triangles for TO phonons in ZnSe. For completeness we also include similar data for a different crystal of GaP as reported by Bairamov *et al.*[19,20]

Note should be taken of the following additional results depicted in Figs. 6 and 7. Namely, (i) the temperature dependence of TO phonon dephasing is less than that of LO dephasing, (ii) the results of the linewidth studies agree among the two experimental groups, and (iii) agreement also exists between the results obtained from the linewidth and from the temporal measurements. It should be further noted that the temporal measurements show quite clearly that the coherent LO phonon state is not destroyed as a result of the dephasing process, rather $\langle Q^2 \rangle$ persists through many orders of $I_c(\Delta t)$ and simply decreases its magnitude exponentially.

B. Third-order nonlinear electronic susceptibility $\chi^{(3)}$

It is clear from Eqs. (1) and (3) that once $\Gamma = 2/T_2$ is determined by the method described above, a further analysis of the full $I_c(\Delta t)$ becomes possible in terms of the integration over the temporal profiles of the laser fields $E_i(t)$, plus an independent evaluation of the Raman tensor element R_A. The result of this procedure leads to a determination of all three nonzero components of $\chi^{(3)}$, of the zinc-blende structure, i.e., χ_{1111}, χ_{1122}, and χ_{1221}.

The first step in this process is to determine in detail the temporal profiles $f_i(t)$ of each laser field $\mathbf{E}_i(t)$. Here, we represent each $\mathbf{E}_i(t)$ by $\theta_i^+(x) f_i(t)$. For this purpose, we have made separate measurements of the $l-l$, $s-s$ laser autocorrelation signal and the l-s laser cross correlation signal. Typical results are shown as the dashed and solid lines in Fig. 5. In the past, various attempts have been made to account for the autocorrelation traces in terms of the following pulse profile functions: (i) Gaussian[21] e^{-t^2}; (ii) Lorentzian[22] $1/(1+t^2)$; (iii) secant hyperbolic[23] $1/\cosh(t) = 2/(e^t + e^{-t})$; and (iv) single-sided exponential[24] $e^{-|t|}$. After substituting each function into the expression for the autocorrelation intensity, the corresponding integration was performed as a function of the time delay width $\Delta t_D(j) = jT_H^{(a)}/4$ where j is an integer from 0 to 12 and $T_H^{(a)}$ is the full width at half maximum (FWHM). The normalized numerical values (with the peak taken at 100%) at each j of $\Delta t_D(j)$ are tabulated in Table I for all four functions. By comparing the numerical values with the corresponding ones obtained experimentally (listed in the second column), the standard variations are calculated and listed in the bottom row. The

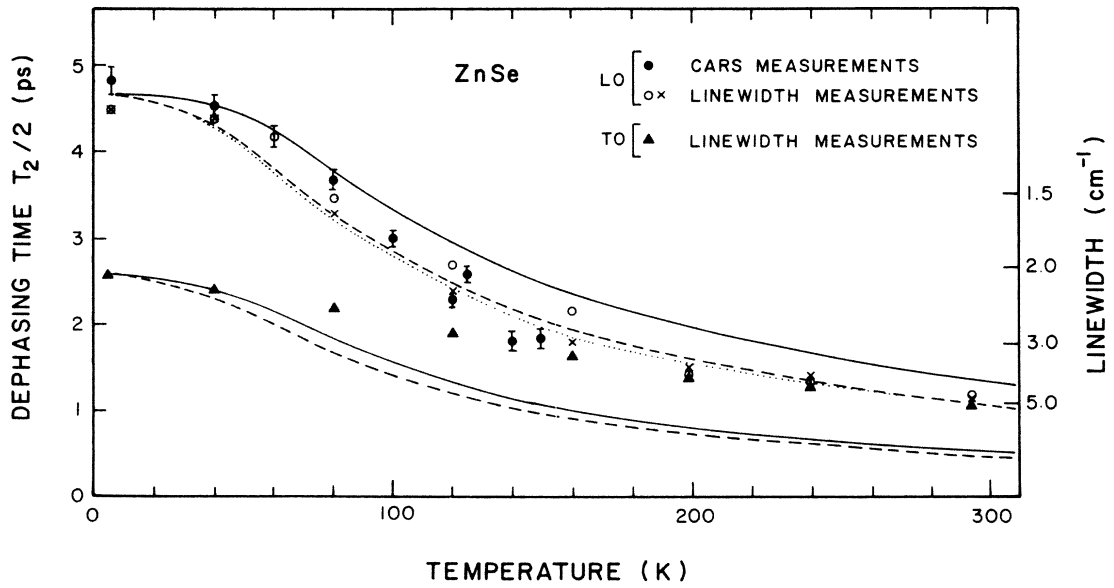

FIG. 7. Temperature dependence of $T_2/2$ and of the Raman linewidth of LO and TO phonons in ZnSe obtained from the present work. For LO phonons the solid line refers to a decay channel terminated at phonons of $\omega_{LA} = \omega_{LO}/2$, the dashed line to terminal phonons with $\omega_{TA} = 2.1$ THz, $\omega_{LA} \sim 5.45$ THz with $\mathbf{q} \sim \pm 0.85$ $(\xi,0,0)$, the dotted line to $\omega_{TA} \sim 1.98$ THz, $\omega_{LA} \sim 5.61$ THz with $\mathbf{q} \sim K$ point. For TO phonons the solid line refers to termination at $\omega_{LA} \sim \omega(\mathrm{TO}/2)$ and the dashed line to $\omega_{TA} \sim 1.95$ THz and $\omega_{LA} \sim 4.14$ THz, $\mathbf{q} \sim \pm 0.5$ $(\xi,0,0)$.

TABLE I. Autocorrelation function.

$\Delta t_D(j)$[a] j	Experimental results	$f(t)$: Pulse profile function e^{-t^2}	$1/\cosh(t)$	$1/(1+t^2)$	$e^{-\lvert t\rvert}$
0	100	100	100	100	100
1	94	95.8	95.5	95.2	93.3
2	81	84.1	83.4	82.6	79.5
3	64	67.7	67.0	66.2	64.2
4	50	50.0	50.0	50.0	50.0
5	39	33.9	35.1	36.3	38.0
6	31	21.0	23.4	25.7	28.4
7	25	12.0	14.9	18.0	20.9
8	19	6.26	9.2	12.7	15.2
9	15	3.0	5.5	8.9	10.9
10	10.5	1.32	3.24	6.38	7.83
11	8.3	0.53	1.87	4.61	5.56
12	6.0	0.2	1.06	3.38	3.93
Standard variation		8.18	6.42	4.14	2.52

[a] $\Delta t_D = T_H^{(a)}/4$.

smallest standard variation is found for the single-sided exponential function. However, since the autocorrelation measurement yields a pulse shape which is symmetric about its maximum for any arbitrary function $f(t)$, an asymmetry of the profile, if it exists, can not be determined through the autocorrelation method alone. In order to determine an asymmetric $f(t)$, the intensity profile of the purely electronic component $I_c^e(\Delta t)$ must be examined. It follows from Eq. (2) that this signal can be expressed as

$$I_c^e(2\omega_l-\omega_s;\Delta t)\propto\int|\bar{\chi}^{(3)}\mathbf{E}_p^+(t-\Delta t)\mathbf{E}_l^+(t)\mathbf{E}_s^-(t)|^2dt \propto\int_{-\infty}^{\infty}|f_p(t-\Delta t)f_l(t)f_s(t)|^2dt\ . \quad (5)$$

Here, it should be noted that $f_p(t)=f_l(t)$, since a portion of the pump beam is used as the probe beam. This expression unlike that for the autocorrelation involves an odd power of the function $f(t)$'s, thus $I_c^e(\Delta t)$ will be asymmetric about its peak (corresponding to $\Delta t=0$) if $f(t)$ is an asymmetric function. The $I_c^e(\Delta t)$ signal, as shown on a $\log_{10}$ intensity scale as the dotted line in Fig. 5, exhibits a distinct asymmetry which reflects the different slopes of the exponentially rising and falling edges of the dye laser pulse. From the above considerations, the function $f(t)$ is described as follows:

$$f(t)=\begin{cases}e^{\gamma^{>}_{\log f}t}, & t\leqq 0\\ e^{-\gamma^{<}_{\log f}t}, & t\geqq 0\end{cases} \quad (6)$$

where $\gamma^{>}_{\log f}$ and $\gamma^{<}_{\log f}$ are the rising and falling slopes of $\log_{10}f(t)$. Moreover, $\gamma^{<}_{\log f}$ and $\gamma^{>}_{\log f}$ can be obtained, respectively, from the slope of the logarithm of the negative and positive time delay sides of $I_c^e(\Delta t)$. Furthermore it has been found, from a large number of experimental observations, that $\delta=\gamma^{>}_{\log f}/\gamma^{<}_{\log f}$ does not change by more than $\pm 4\%$. We find throughout that $\delta=1.3\pm0.05$ and, hence, will use this value in what follows. The dashed curve given in Fig. 5 shows a fit to a particular autocorrelation signal with $\gamma^{<}_{\log f}=0.3\ \text{ps}^{-1}$. Because it is impossible to set the laser pulse duration (which depends on $\gamma^{<}_{\log f}$) to the same value throughout the experiment, the parameter $\gamma^{<}_{\log f}$ must be independently determined for each run.

The asymmetric profile can not, however, on its own explain the broadening of the cross correlation (solid line) compared to autocorrelation signal (dashed line) in Fig. 5. This property can be accounted for by a random temporal fluctuation (so-called "jitter") between the l and s lasers. Length variations of the dye laser cavities due to irregular flow in the dye jet, thermal and mechanical instabilities of the cavity, and fluctuation of the pump pulse train are suspected as the main sources of the jitter.[1]

We assume the jitter to possess a Gaussian temporal profile, and since the final $I_c(\Delta t)$ involves the product of the three fields $\mathbf{E}_l$, $\mathbf{E}_s$, $\mathbf{E}_p$ we shift, for convenience, the resulting broadening totally on to $\mathbf{E}_s$. In an analogous manner to the autocorrelation signal, we find a good fit for the cross correlation profile (see solid line in Fig. 5) by using a broadened temporal function, $f_s'(t)$, for the s laser as follows:

$$f_s'(t)=\begin{cases}Be^{\gamma^{>}_{\log f}t}-be^{z\gamma^{>}_{\log f}t}, & t\leqq 0\\ Be^{-\gamma^{<}_{\log f}t}-be^{-z\gamma^{<}_{\log f}}, & t\geqq 0\end{cases} \quad (7)$$

where $B=1/(1-1/z)$, $b=B-1$, and $z(>1)$ is the broadening parameter which must be determined from the experiment. Here, we have taken advantage of the expansion for small values of t of the Gaussian profile $e^{-\kappa t^2}$. The corresponding cross correlation function as compared to the experimental result is given in Table II. The standard variation is found to be 1.2 as compared to that for a full Gaussian jitter of 0.5. We claim no inherent physical significance for $f_s'(t)$ except that it does yield good agreement with the data, and that it permits analytical integration of Eq. (3).

Finally, the unavoidable small temporal mismatch between the l and s lasers (at $\Delta t=0$) leads to the introduction of another parameter δt. The corresponding overlap function becomes for the case of $\delta t\leqq 0$,

TABLE II. Cross correlation function.

$\Delta t_D(j)$[a] j_0	Experimental results 100	Gaussian jitter 100	$f'(t)$ 100
1	95	95	95
2	83	83	82
3	66	67	66
4	50	50	50
5	35	36	37
6	24	24	25
7	16	16	17
8	10	10	12
9	6	6	7
10	4	4	5
Standard variation		0.5	1.2

[a] $\Delta t_D(4)=T_H^{(c)}$.

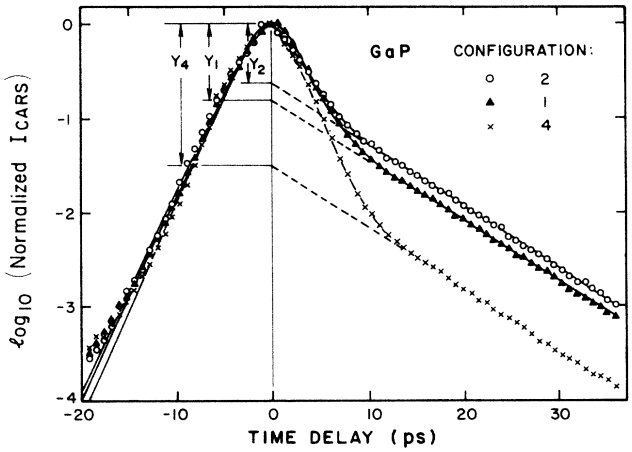

FIG. 8. Experimental data (symbols) for GaP and fitted $I_c(\Delta t)$ (solid line) for each of the polarization configurations indicated in the insert to the figure and defined in Fig. 3. The data were first reported in Ref. 2.

$$f_{ls}(f,\delta t)=f_l(t)f_s'(t,\delta t)=\begin{cases} Be^{-\gamma_{\log f}^{>}\delta t}e^{2\gamma_{\log f}^{>}t}-be^{-z\gamma_{\log f}^{>}\delta t}e^{(1+z)\gamma_{\log f}^{>}t}, & -\infty<t\leq\delta t \\ Be^{\gamma_{\log f}^{<}\delta t}e^{(\gamma_{\log f}^{>}-\gamma_{\log f}^{<})t}-be^{z\gamma_{\log f}^{<}\delta t}e^{(\gamma_{\log f}^{>}-z\gamma_{\log f}^{<})t}, & \delta t\leq t\leq 0 \\ Be^{\gamma_{\log f}^{<}\delta t}e^{-2\gamma_{\log f}^{<}t}-be^{z\gamma_{\log f}^{<}\delta t}e^{-(1+z)\gamma_{\log f}^{<}t}, & 0\leq t<\infty\ . \end{cases} \tag{8}$$

In order to derive an explicit expression for $I_c(\Delta t)$ in Eq. (3), it is necessary to solve Eq. (1) subject to the temporal overlap condition of Eq. (8), i.e.,

$$\mu(\ddot{Q}^{+}+\Gamma\dot{Q}^{+}+\omega_{\mathrm{LO}}^2Q^{+})=R_A\{j\}\theta_l^{+}\theta_s^{-}f_{ls}(t,\delta t)\ . \tag{9}$$

Then, its solution can be written as[11]

$$Q^{+}=\frac{R_A\{j\}\theta_l^{+}\theta_s^{-}}{\mu\omega_{\mathrm{LO}}\Gamma}f_Q(t)\ , \tag{10}$$

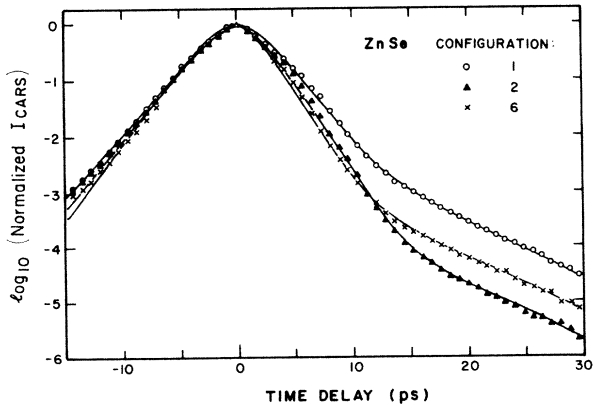

FIG. 9. Same as Fig. 8, except for ZnSe. The data have not been previously reported.

where $f_Q(t)$ represents the transient behavior of the coherent LO phonons, which is independent of configuration. The algebra manipulation necessary to obtain $f_Q(t)$, plus those necessary to obtain the nonlinear polarization P_{NL} and the subsequent derivation of $I_c(\Delta t)$ have been carried out elsewhere.[11] Typical best fit curves obtained for GaP and ZnSe are drawn as solid lines in Figs. 8 and 9 and the numerical results from 28 runs spread over the seven configurations are listed for GaP in Table III and from 19 runs over seven configurations are listed for ZnSe in Table IV. Note should be taken that the values in Table III for GaP differ somewhat from those presented in Ref. 3. This stems from an algebraic error present in the formulation used in Ref. 3, which has now been corrected.

TABLE III. Components of $\chi^{(3)}$ for GaP (10^{-10} esu unit).

$\chi'_{1122}=2.3\pm0.3$
$\chi''_{1122}=-0.8\pm0.8$
$\chi'_{1221}=2.9\pm0.2$
$\chi''_{1221}=-0.7\pm0.3$
$\chi'_{1111}=1.7\pm0.5$
$\chi''_{1111}=-0.3\pm1.1$

TABLE IV. Components of $\chi^{(3)}$ for ZnSe (10^{-11} esu unit).

$\chi'_{1122}=9.1\pm1.6$
$\chi''_{1122}=-4.0\pm1.4$
$\chi'_{1221}=6.9\pm0.5$
$\chi''_{1221}=-1.7\pm2.0$
$\chi'_{1111}=9.2\pm1.9$
$\chi''_{1111}=-4.6\pm3.0$

V. DISCUSSION

As noted in Sec. II, the dephasing time $T_2/2$ may include contributions from all dephasing phenomena such as elastic scattering from crystal surfaces, from impurities, from imperfections, from electronic carriers, and from phonon-phonon scattering.

We have left until this point a discussion of possible effects of lattice imperfections on our results. Whatever the effect is on the dephasing rate, to a good approximation, we can assume it to be temperature independent in comparison to that of anharmonic phonon-phonon scattering, since the former is proportional to $n_T(\omega_{\rm LO})$ (Ref. 16) as compared to the latter which is proportional to $2n_T(\omega_{\rm LA})$ (see Eq. 4).

In the low-temperature regime, for which $\hbar\omega \gg k_B T$, three phonon interactions should dominate.[25] Of the possible interactions only LO phonon decay into acoustic phonons (and their recombination) needs be considered. Combination of a longitudinal optical phonon at the zone center with an acoustic phonon cannot occur since this would produce a phonon with $\omega > \omega_{\rm LO}(q \approx 0)$ which cannot exist in GaP. Moreover, the phonon dispersion relations of GaP,[26] plus energy and crystal momentum considerations, rule out all interactions except

$$\mathrm{LO}(\omega_{\rm LO},0) \leftrightarrow \mathrm{LA}(\omega_{\rm LO}/2,\mathbf{q}') + \mathrm{LA}(\omega_{\rm LO}/2,-\mathbf{q}') \ .$$

Here, $\mathbf{q}'$ is the wave vector of the LA phonon at half the LO phonon energy. We shall refer to this interaction as the "Klemens's channel."[27]

If only the Klemens's channel is considered the expression Eq. (4) for the population decay time (τ) can be further simplified to

$$\tau(T)=\frac{1}{\Gamma}=\frac{\tau_0}{1+2n_T(\omega_{\rm LO}/2)} \ , \tag{11}$$

where τ_0 is the population decay time at zero temperature. Hence, the general dephasing time becomes

$$\frac{2}{T_2}=\frac{1}{T_{\rm im}}+\frac{1+2n_T(\omega_{\rm LO}/2)}{\tau_0} \ , \tag{12}$$

where $T_{\rm im}$ is the dephasing time due to scattering from imperfections.

The solid curve given in Fig. 6 indicates the temperature variation of the dephasing time for GaP as obtained from Eq. (12) with the following best fit values for $T_{\rm im}=\infty$ and for $\tau_0=24.6$ ps. Thus impurity scattering does not play an important role even in the presence of nitrogen impurities of the order of $10^{16}/\mathrm{cm}^3$ in our crystal of GaP.

In the case of ZnSe, the phonon dispersion relations[26] indicate several possible decay channels in addition to Klemens' decay channel. For example, along the [100] direction, decay to TA (~ 70 cm^{-1}) and LA (~ 181 cm^{-1}) phonons conserves energy and crystal momentum. The expected temperature dependence of $T_2/2$ for these cases are also indicated in Fig. 7, as in the case of the Klemen's channel, we find a best fit with $T_{\rm im}=\infty$ and $\tau_0=4.5$ ps (see solid line). The experimental observation, in both GaP and ZnSe, of a more rapid decay with increasing temperature than that predicted by Klemens implies that higher order phonon-phonon interactions are beginning to play a role. Since it is impossible at this time to enumerate all the possible decay channels and the corresponding strengths accurately due to insufficient knowledge of the third order anharmonic potential,[28,29] a complete analysis of the dephasing time including its absolute value will not be attempted.

Particular note should be taken that when the observed dephasing time obtained from the Raman linewidth measurements is compared to that from the CARS measurements, it is found that the two different methods yield identical results within experimental error. This observation has been forshadowed by previously derived theoretical expressions for $T_2/2$ for each case which are also found to be identical in every way.[16,17] These predictions assume, as is the case here, that the acoustic phonons produced in the decay of the LO phonons do not appreciably increase $n(\omega_{\rm LA})$ beyond its value at thermal equilibrium $n_T(\omega_{\rm LA})$. It remains to be seen what happens when $n(\omega_{\rm LA}) \gg n_T(\omega_{\rm LA})$ for which phonon breakdown[30] and phonon renormalization[31] effects have been predicted to be of importance. Moreover, note should be taken that the observed exponential decay of the TRCARS intensity (see Figs. 4, 8, and 9) implies that during this process the overall coherent state is not destroyed but merely diminished.

Figures 6 and 7 also display the temperature dependence of the decay of near-zone-center TO phonons. It is clear that the experimental results are not in agreement with the predictions of Eq. (12). This is particularly so for TO phonons in GaP for which $T_2/2$ is found to be independent of temperature over the range 5—300 K, whereas $T_2/2$ for ZnSe has a much lower than expected temperature dependence. Curiously, similar data for TO phonons in GaAs (Ref. 32) obey Eq. (12), suggesting that the temperature dependence of $T_2/2$ for TO phonons, particularly in GaP, and to a lesser extent in ZnSe, is anomalous. Barker[33] has pointed out that the line shape of the spontaneous Raman scattering intensity for TO phonons in GaP is asymmetric and not Lorentzian, and has suggested that this results from anharmonic decay of TO ($q \sim 0$) into a nearly degenerate continuum of decay channels terminating at TA and LA states near the X point in the Brillouin zone. Weinstein[34] has shown that the asymmetry can be removed by hydrostatic pressure, and proposes that this results from different pressure shifts of the TO ($q \sim 0$) state and TA + LA(X) state, thereby, removing the near degeneracy present at atmospheric pressures. We postulate that a similar mechanism

is responsible for our results. We suggest that the combined density of state of the $TO(q\sim 0)\leftrightarrow TA+LA(X)$ continuum is larger at liquid helium temperatures than at higher temperatures, thus the expected decrease in $T_2/2$ with temperature is compensated by the statistical factors in Eq. (12). Verification of this postulate must await, however, careful determination of the phonon dispersion relations of GaP at various temperature and a calculation of the temperature dependence of the combined density of states.

We have previously discussed[3] the role of two-photon absorption on the complex component of $\chi^{(3)}$ and on the advantages and disadvantages of the determination of $\chi^{(3)}$ from measurements in the time domain to those performed in the spectral domain. Here we address the trends in the response coefficients, i.e., $\chi_R^{(3)}$ and $\chi_{\text{eff}}^{(3)}$, which are discernible from the experimental results. Since at this point, only a very limited set of III-V semiconductors have been investigated, and since the results depend on the laser frequencies, i.e., ω_l and ω_s, the following observations must be taken with considerable caution. According to Eq. (3) the relative intensity I_{rel} at $\Delta t=0$, of the vibrational component to the electronic component of $I_c(\Delta t)$ depends qualitatively on the ratio $|R_A/\chi_{\text{eff}}^{(3)}|^2$. Thus, I_{rel} is predicted roughly to be proportional to $\sim 4\times 10^{22}$ ($\text{Å}^2/\text{esu}^2$) for GaP, and to $\sim 5\times 10^{21}$ ($\text{Å}^2/\text{esu}^2$) for ZnSe. In other words, all else being equal, the intercept of the vibrational part of the normalized I_c at $\Delta T=0$ for GaP (see Fig. 4) should be roughly one order of magnitude larger than the corresponding intercept for ZnSe. This is, of course, observed experimentally. As is well known,[13] the strength of the Raman cross-section is some function of the difference between the excitation frequency and the Raman resonances frequency. Far enough from a resonance, we expect a similar dependence of $\chi_{\text{eff}}^{(3)}$ on the ratio of the (squared) laser frequencies and the (squared) electronic gap energy of the semiconductor. That is, all else (such as laser frequencies ~ 2.28 eV) being equal, we expect $\chi_{\text{eff}}^{(3)}$ to be smaller for ZnSe (minimum gap ~ 2.8 eV at 4 K) compared to GaP (minimum gap ~ 2.4 eV at 4 K). Thus we predict roughly that $\chi_{\text{eff}}^{(3)}$ of ZnSe is ~ 0.2 times that of GaP, whereas we observe the ratio of average values to be 0.15. It remains to be seen if these simple, essentially qualitative rules, will apply to a larger set of III-V compounds.

VI. CONCLUSIONS

In this paper, the decay processes of coherent LO phonons (near zone center) are investigated experimentally. By using mode-locked picosecond lasers, the dephasing time of the coherent LO phonons in GaP and ZnSe was measured directly in the time domain as a function of temperature from 5 to 300 K and compared to that from conventional spontaneous Raman linewidth measurements. It is found that the decay time obtained from the two different methods is the same. Especially for GaP, the observed change in the dephasing time with temperature correlates very well with the theory of cubic anharmonic processes developed by Maradudin and Fein,[17] provided that LO phonons decay into two half-energy LA phonons with equal but opposite wave vectors. Moreover, in an experiment to be reported elsewhere[4] we find, through vibronic phonon sideband measurements performed in the presence of highly populated coherent LO phonons, anti-Stokes luminescence intensities due solely to the decay of coherent LO phonons (403 cm^{-1}) into LA phonons (201.5 cm^{-1}). Thus we demonstrate the first experimental proof that the simple third-order decay postulated by Klemens[27] dominates dephasing of coherent LO phonons in the low-temperature regime. Moreover, we find for acoustic phonon populations of the order of thermal populations that anharmonic interactions do not disturb the coherent LO phonon states, but merely diminish the coherent intensity.

On the other hand, since the coherent LO phonon state is associated with a nonlinear polarization, it can be used to study the nonlinear optical properties of solids. By analyzing the characteristics of the CARS intensity in the time domain the three active components of the third order nonlinear susceptibility, $\chi_b^{(3)}$, due to bound electrons in GaP and ZnSe are determined for the first time. For this purpose, it is necessary to determine the temporal profiles of the pulses of the exciting picosecond dye lasers. These profiles are found to be very well approximated by an asymmetric single-sided exponential function.

The temporal method employed here is complementary to the spectral method developed by Levenson *et al.*,[9] i.e., the temporal method must be used to determine $\chi_b^{(3)}$ when a material parameter $\xi\approx\chi_{\text{eff}}^{(3)}/\chi_R^{(3)}\gg 1$ whereas the spectral method must be used in the opposite limit. Experiments in the time domain are promising tools in the study of the frequency dispersion of $\chi_b^{(3)}$, particularly as the spectrum covered by picosecond dye lasers is constantly being expanded and their stability improved.

ACKNOWLEDGMENTS

The authors (W.E.B. and B.K.R.) acknowledge support through ARO DAAG29-83-K-0091 and wish to thank the Max Planck Institut-FKF for their kind hospitality.

APPENDIX: EFFECTIVE THIRD-ORDER SUSCEPTIBILITIES

The derivation of the effective $\chi^{(3)}$ for the various polarization conditions in Fig. 2 has been carried out elsewhere.[11] There are two contributions $\chi_R^{(3)}$ and $\chi_{\text{eff}}^{(3)}$. The first of these components corresponds to the response of the vibrational system and is related to the first term in the square brackets in Eq. (3), whereas the second component corresponds to the electronic response and to the second term in the square brackets in Eq. (3).

The explicit expressions for $\chi_R^{(3)}$ and $\chi_{\text{eff}}^{(3)}$ are the following:

(a) Configuration 1:

$$\chi_R^{(3)}\{1\}=NR_AR_\chi/\Gamma$$

and (A1)

$$\chi_{\text{eff}}^{(3)}\{1\}=3\chi_{1221}^{(3)}$$

TABLE V. Physical parameters.

	GaP	ZnSe
N (10^{22}/cm^3)	2.47	2.19
μ (10^{-23} g)	3.59	5.95
$\hbar\omega_0$ (cm^{-1})	367[a]	204[b]
$\hbar\omega_l$ (cm^{-1})	403[a]	251[b]
R_A(LO) (10^{-15} cm^2)	2.5[c]	0.7[c]
$\chi^{(2)}$ (10^{-7} esu)	3.4[d]	1.96[e]

[a]Reference 35.
[b]Reference 36.
[c]Reference 13.
[d]Reference 37.
[e]Reference 38.

TABLE VI. Polarization configurations.

Configuration	$S\{j\}$	$\xi\{j\}R_0/3$
1	1	χ_{1221}
2	1	χ_{1122}
3	$\frac{1}{2}$	$2\chi_{1122}$
4	1	$(\chi_{1111}+\chi_{1221}+2\chi_{1122})/2$
5	$\frac{1}{2}$	$\chi_{1111}+\chi_{1221}$
6	$\frac{1}{2}$	$\chi_{1111}+\chi_{1122}$
7	$\frac{1}{2}$	$\chi_{1122}+\chi_{1221}$

in which $R_\chi=R_A/(\mu\omega_{\rm LO})$ and the numerical values can be obtained from Table V.

(b) Configuration 2:

$$\chi_R^{(3)}\{2\}=NR_AR_\chi/\Gamma$$

and (A2)

$$\chi_{\rm eff}^{(3)}\{2\}=3\chi_{1122}^{(3)} .$$

(c) Configuration 3:

$$\chi_R^{(3)}\{3\}=NR_AR_\chi/2\Gamma$$

and (A3)

$$\chi_{\rm eff}^{(3)}\{3\}=3\chi_{1122}^{(3)} .$$

(d) Configuration 4:

$$\chi_R^{(3)}\{4\}=NR_AR_\chi/\Gamma$$

and (A4)

$$\chi_{\rm eff}^{(3)}\{4\}=\tfrac{3}{2}(\chi_{1111}^{(3)}+\chi_{1221}^{(3)}+2\chi_{1122}^{(3)}) .$$

(e) Configuration 5:

$$\chi_R^{(3)}(5)=NR_AR_\chi/2\Gamma$$

and (A5)

$$\chi_{\rm eff}^{(3)}\{5\}=\tfrac{3}{2}(\chi_{1111}^{(3)}+\chi_{1221}^{(3)}) .$$

(f) Configuration 6:

$$\chi_R^{(3)}\{6\}=NR_AR_\chi/2\Gamma$$

and (A6)

$$\chi_{\rm eff}^{(3)}\{6\}=\tfrac{3}{2}(\chi_{1111}^{(3)}+\chi_{1122}^{(3)}) .$$

(g) Configuration 7:

$$\chi_R^{(3)}\{7\}=NR_AR_\chi/2\Gamma$$

and (A7)

$$\chi_{\rm eff}^{(3)}\{7\}=\tfrac{3}{2}(\chi_{1122}^{(3)}+\chi_{1221}^{(3)}) .$$

By defining a constant R_0,

$$R_0=NR_AR_\chi ,$$

the total nonlinear polarization, $P_{\rm NL}^{(3)}$, can be rewritten in a convenient form;

$$P_{\rm NL}^{(3)+}\{j\}=S\{j\}R_0[f_Q(t)/\Gamma+\xi\{j\}f_l(t)f_s(t)] \times f_p(t-\Delta t)\theta_p^+\theta_l^+\theta_s^- , \quad \text{(A8)}$$

where

$$S\{j\}=\chi_R^{(3)}\{j\}\Gamma/R_0$$

and

$$\xi\{j\}=\chi_{\rm eff}^{(3)}\{j\}/(S\{j\}R_0) .$$

According to these definitions, the corresponding values for each configuration have been tabulated in Table VI.

*Present address: Department of Physics, University of California at Irvine, Irvine, CA 92717.
†Present address: Optical Sciences Center of the University of Arizona, Tucson, AZ 85721.

[1]J. Kuhl and D. von der Linde, in *Picosecond Phenomena III*, edited by K. B. Eisenthal, R. M. Hochstrasser, W. Kaiser, and A. Laubereau (Springer, Berlin, 1982), pp. 201–204.
[2]J. Kuhl and W. E. Bron, Solid State Commun. **49**, 935 (1984); Physica **117B/118B**, 532 (1983).
[3]B. K. Rhee, W. E. Bron, and J. Kuhl, Phys. Rev. B **30**, 7358 (1984).
[4]B. K. Rhee and W. E. Bron, Phys. Rev. B **34**, 7107 (1986).
[5]See, e.g., W. Demtroeder, *Laser Spectroscopy* (Springer, Berlin, 1981).
[6]In reality the number of excited modes is larger than the ideal one due to unavoidable optical focusing effects and due to uncertainty effects resulting from the short duration of the laser pulses.
[7]E. Garmire, F. Panderese, and C. H. Townes, Phys. Rev. Lett. **11**, 160 (1963).
[8]T. A. Giordmaine and W. Kaiser, Phys. Rev. **144**, 676 (1966).
[9]M. D. Levenson and N. Bloembergen, Phys. Rev. B **10**, 4447 (1974).
[10]L. L. Schiff, *Quantum Mechanics*, third edition (McGraw-Hill, New York, 1968). See, also, W. A. Harrison, *Solid State Physics* (McGraw-Hill, New York, 1970), pp. 408ff.

[11]Unpublished thesis submitted to Indiana University by B. K. Rhee as partial requirement for the Ph.D. degree, September 1985. A full derivation of the pertinent components of the intensity of the CARS signal, plus the reduction of the data to obtain the third-order nonlinear susceptibilities appear in this thesis. A copy of the derivation and the computer algorithms are presented in the thesis. The thesis is available through University Microfilm International (Ann Arbor, Michigam 48106).

[12]S. Ushioda, A. Pinczuk, E. Burstein, and D. L. Mills, in *Light Scattering Spectra of Solids,* edited by G. B. Wright (Springer, New York, 1969), pp. 347.

[13]J. M. Calleja, H. Vogt, and M. Cardona, Philos. Mag. A **45**, 239 (1982).

[14]Chr. Flytzanis and N. Bloembergen, Prog. Quant. Electron. **4**, 271 (1976).

[15]See D. von der Linde, J. Kuhl, and H. Klingenberg, Phys. Rev. Lett. **44**, 1505 (1980); J. A. Kash, J. C. Tsang, and J. M. Hvam, Phys. Rev. Lett. **54**, 2151 (1985) and references cited therein.

[16]P. Carruthers and K. S. Dy, Phys. Rev. **147**, 214 (1966).

[17]A. A. Maradudin and A. E. Fein, Phys. Rev. **128**, 2589 (1962).

[18]See, e.g., A. Laubereau and W. Kaiser, Rev. Mod. Phys. **50**, 607 (1978).

[19]B. Kh. Bairamov, D. A. Parshin, V. V. Toporov, and Sh. B. Ubaidullav, Pis'ma Zh. Tekh. Fiz. **5**, 1116 (1979) [Sov. Techn. Phys. Lett. **5**, 466 (1979)].

[20]B. Kh. Bairamov, Yu. E. Kitaev, V. K. Negoduiko, and Z. M. Kashkhozhev, Fiz. Tverd. Tela (Leningrad) **16**, 2036 (1974) [Sov. Phys.—Solid State **16**, 1323 (1975)].

[21]C. K. Chan, S. O. Sari, and R. F. Foster, J. Appl. Phys. **47**, 1139 (1976).

[22]J. A. Armstrong, Appl. Phys. Lett. **10**, 16 (1967).

[23]H. A. Haus, IEEE J. Quantum Electron. **QE-11**, 736 (1975).

[24]E. P. Ippen and C. V. Shank, Appl. Phys. Lett. **27**, 488 (1975).

[25]R. Orbach and L. A. Vredevoe, Physics **1**, 91 (1964).

[26]H. Bilz and W. Kress, *Phonon Dispersion Relations in Insulators* (Springer, Berlin, 1979).

[27]P. G. Klemens, Phys. Rev. **148**, 845 (1966).

[28]A. S. Pine and P. E. Tannenwald, Phys. Rev. **178**, 1424 (1968).

[29]T. R. Hart, R. L. Aggrawal, and B. Lax, Phys. Rev. B 1, 638 (1970).

[30]R. Orbach, IEEE Trans. Sonics Ultrason. **SU-14**, 140 (1967).

[31]S. A. Bulgadaev and I. B. Levinson, Zh. Eksp. Teor. Phys. **67**, 2341 (1974) [Sov. Phys.—JETP **40**, 1161 (1974)].

[32]R. K. Chang, J. M. Ralston, and D. E. Keating, in *Light Scattering Spectra in Solids,* edited by G. B. Wright (Springer, New York, 1969), pp. 369.

[33]A. S. Barker, Phys. Rev. **165**, 917 (1968).

[34]B. A. Weinstein, Solid State Commun. **20**, 999 (1976).

[35]A. Moordian and G. B. Wright, Solid State Commun. **4**, 431 (1966).

[36]M. Krauzman, C. R. Acad, Science (Paris) **264**, 1117 (1967).

[37]W. L. Faust and C. Henry, Phys. Rev. Lett. **17**, 1265 (1966).

[38]D. J. Bradley and A. J. F. Durrant, Phys. Lett. **27A**, 73 (1968).